

Supporting Information

Bimetallic Sulfide $\text{Sb}_2\text{S}_3@\text{FeS}_2$ Hollow Nanorods as High-Performance Anode Materials for Sodium-Ion Batteries

Liang Cao,[‡] Xuanwen Gao,[§] Bao Zhang,[‡] Xing Ou^{,‡} Jiafeng Zhang,[‡] Wen-Bin Luo^{*,§}*

[‡] School of Metallurgy and Environment, Central South University, No.932 South Lushan Road, Changsha, Hunan 410083, P. R. China

[§] Institute for Energy Electrochemistry and Urban Mines Metallurgy, School of Metallurgy, Northeastern University, No. 11 Lane 3, Wenhua Road, Shenyang, Liaoning, 110819, P. R. China

Corresponding Authors

E-mail: ouxing@csu.edu.cn (X. Ou);

luowenbin@smm.neu.edu.cn (W.-B. Luo)

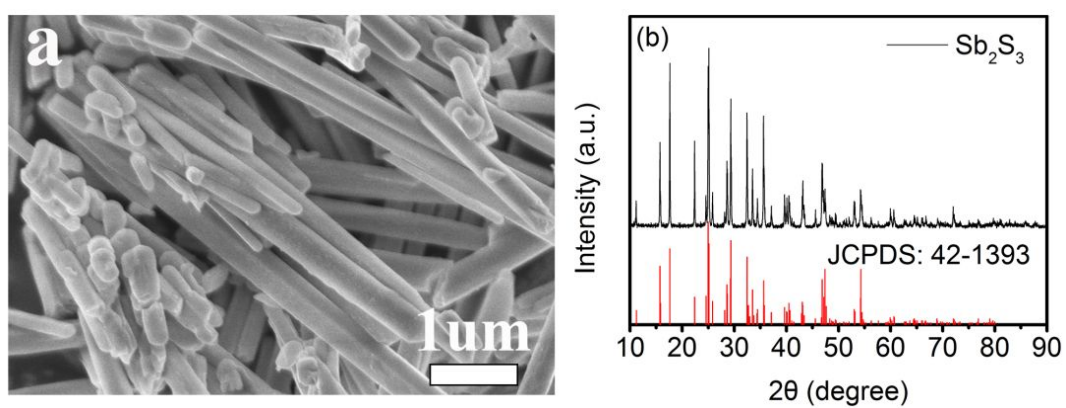


Figure S1. SEM image (a) and XRD pattern (b) of Sb_2S_3 nanorod precursor.

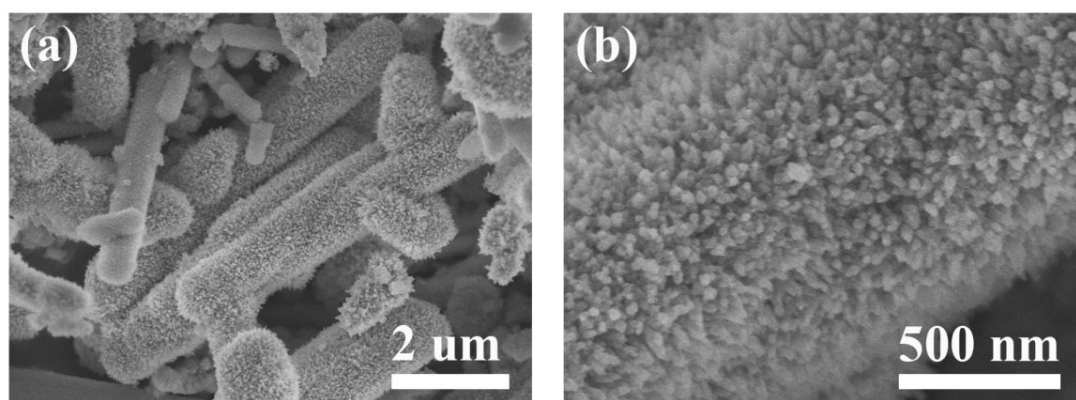


Figure S2. Pristine (a) and magnified (b) SEM images of $\text{Sb}_2\text{S}_3@Fe_2O_3$ precursor.

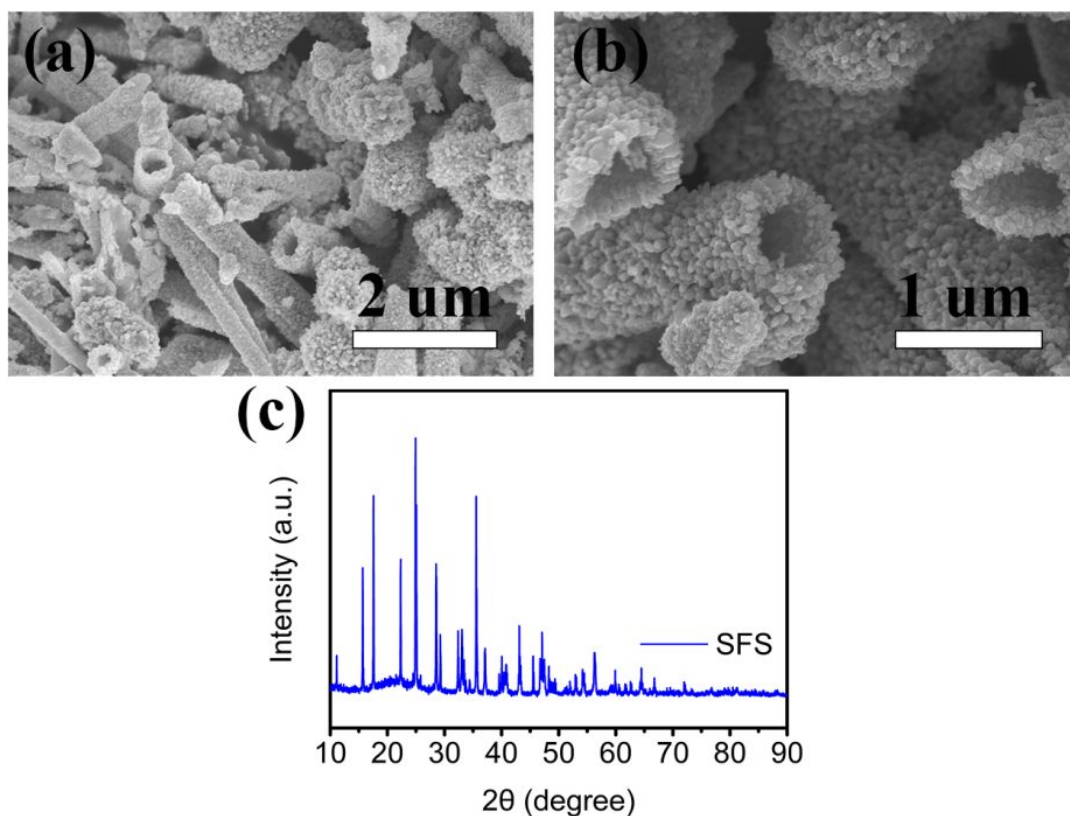


Figure S3. Pristine (a) and magnified (b) SEM images of SFS composite. XRD pattern of SFS composite (c).

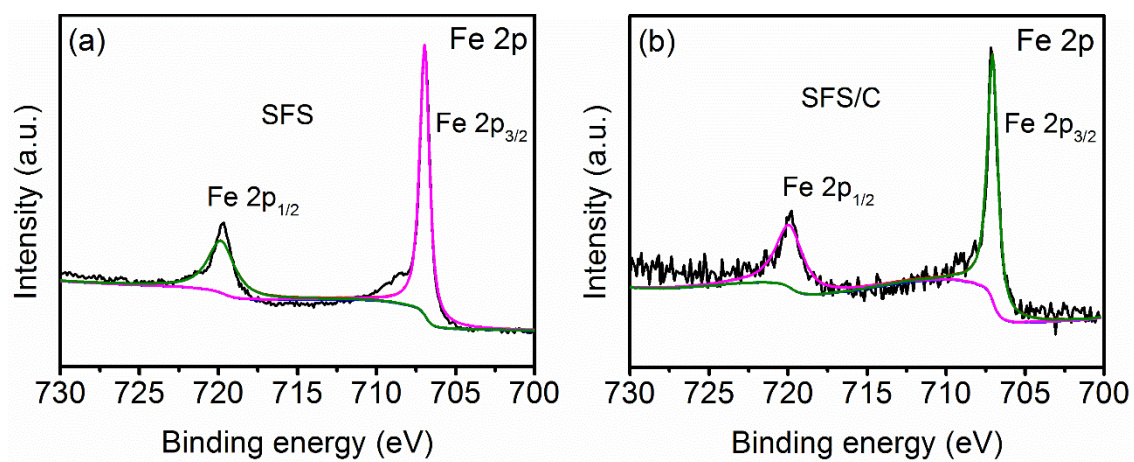


Figure S4. High-resolution Fe 2p XPS spectra for SFS (a) and SFS/C (b) composites.

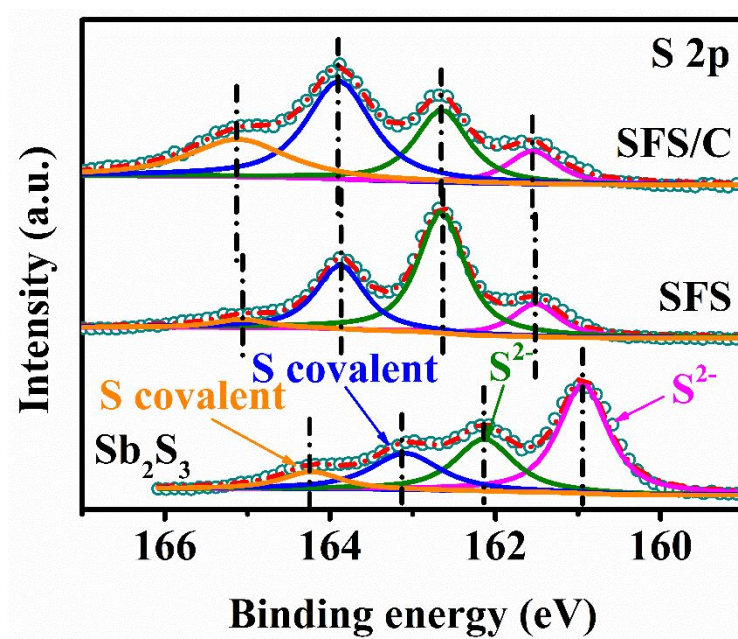


Figure S5. High-resolution S 2p XPS spectra for Sb₂S₃, SFS and SFS/C electrodes.

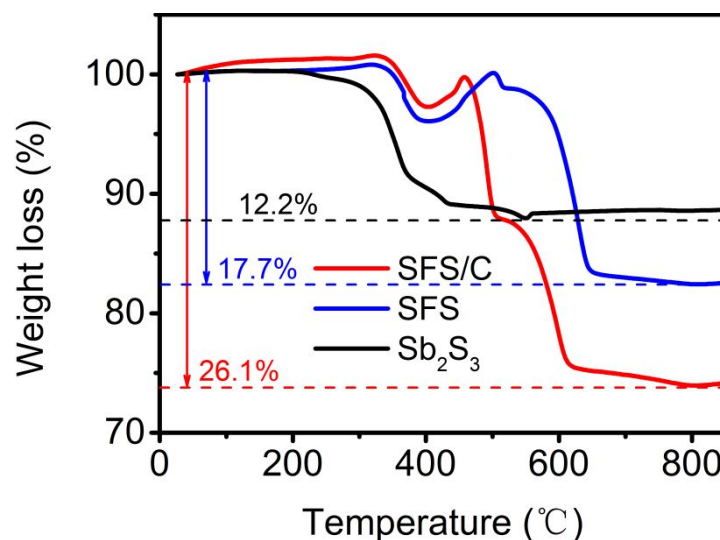


Figure S6. The TGA analysis of SFS/C, SFS and Sb₂S₃ composites.

For the SFS/C electrode, the initial weight loss between 300 and 400°C is attributed to the combustion of Sb₂S₃ with the formation of Sb₂O₄.^{S1} The following two stages of weight loss in the range of 400-600 °C can be assigned to the combustion of carbon in air and the oxidation of FeS₂ to Fe₂O₃, respectively.^{S2} It is worth noting that the weight increase at around 400°C may be indexed into the formation of FeSO₄.^{S3} The content of the graphene is calculated to be $\approx 10.2\%$.

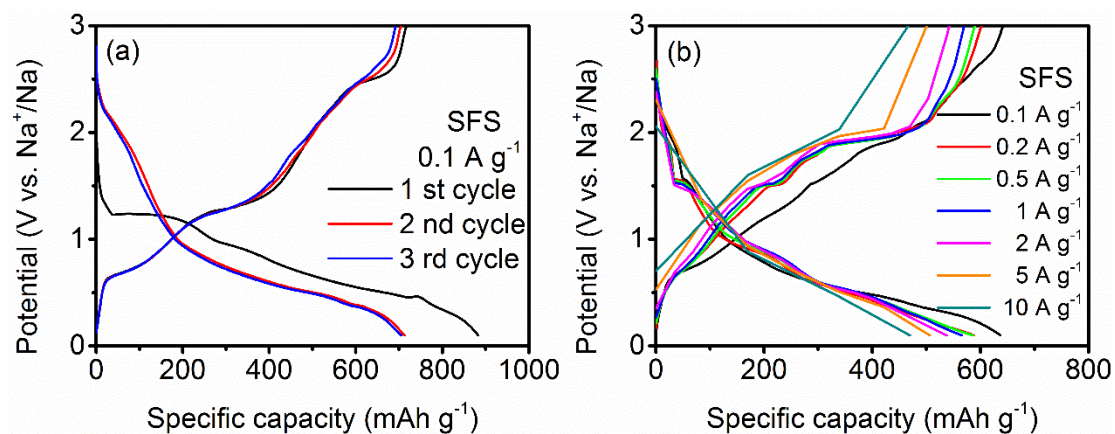


Figure S7. The charge/discharge curves during the initial three cycles at 0.1 A g⁻¹ (a), and at different current densities from 0.1 to 10 A g⁻¹ (b) for SFS electrode.

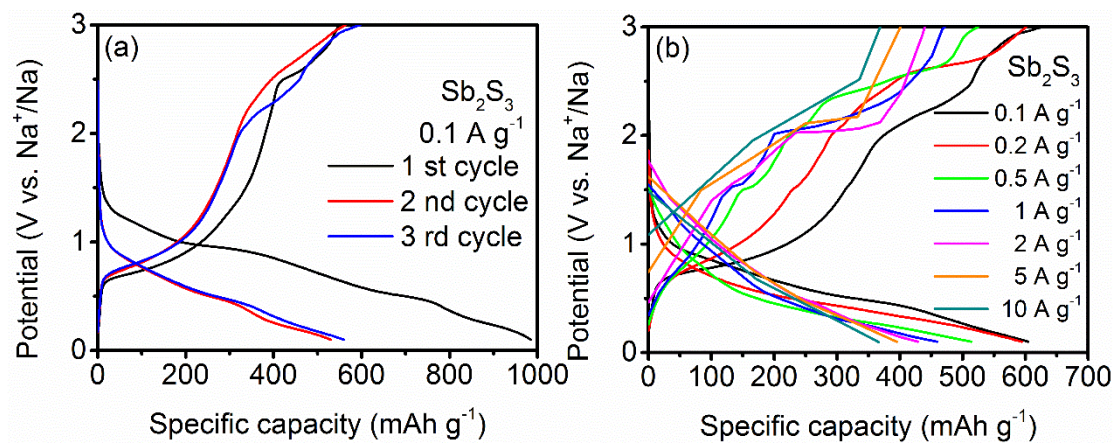


Figure S8. The charge/discharge curves during the initial three cycles at 0.1 A g⁻¹ (a), and at different current densities from 0.1 to 10 A g⁻¹ (b) for Sb₂S₃ electrode.

Table S1. Comparison of the cycling stability of SFS/C with other reported Sb₂S₃-based anodes for SIBs.

Sample	Current density (mA g ⁻¹)	Cycle number	Reversible capacity (mAh g ⁻¹)	References
MWNTs@Sb ₂ S ₃ @PPy	100	100	596	S1
IL-Sb ₂ S ₃ /rGO	500	100	495.1	S2
ZnS-Sb ₂ S ₃ @C	100	120	630	S4
SnS ₂ /Sb ₂ S ₃ @rGO	1000	400	513	S5
Sb ₂ S ₃ /PPy	500	50	236	S6
Sb ₂ S ₃ /MoS ₂	100	100	610	S7
Sb ₂ S ₃ @MWCNTs	50	50	412.3	S8
Sb ₂ S ₃ @C	100	100	699.1	S9
Sb ₂ S ₃ @P/C	50	100	611	S10
SSNR/C	100	100	570	S11
rGO/ Sb ₂ S ₃	50	50	670	S12
a- Sb ₂ S ₃	50	100	586	S13
SFS/C	5000	1000	534.8	This work
SFS	5000	600	518.9	This work

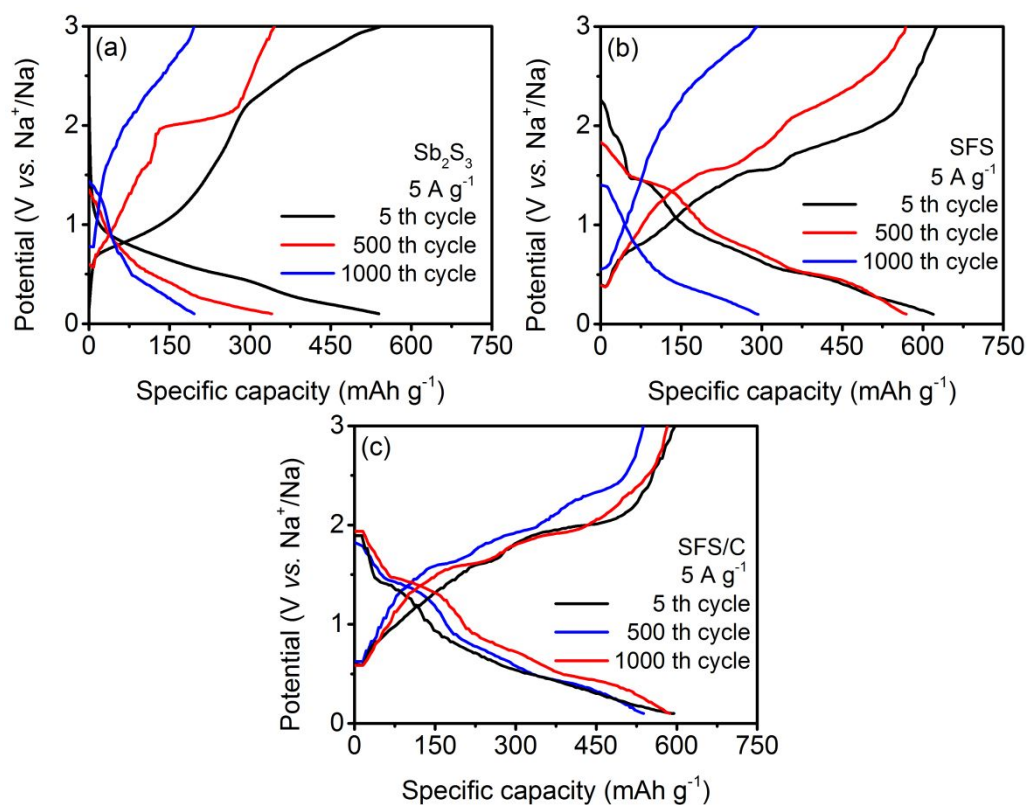


Figure S9. The charge/discharge curves at ultrahigh rate of 5 A g⁻¹ at different cycles for Sb₂S₃ (a), SFS (b), and SFS/C (c) composites.

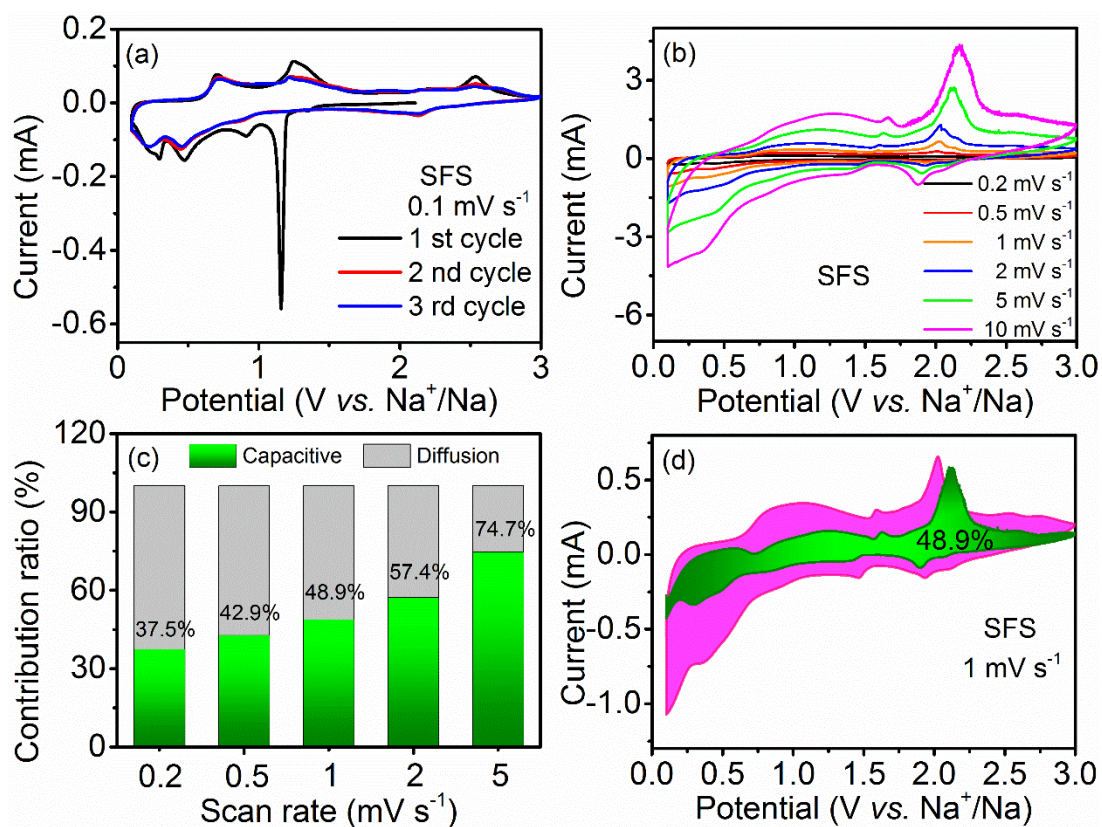


Figure S10. The CV curves at a scan rate of 0.1 mV s^{-1} during the initial three cycles (a), and at different scan rates (b) for SFS composite. The proportion of capacity contribution at different scan rates (c) and the CV curves with the pseudocapacitive contribution at 1.0 mV s^{-1} (d) for SFS composite.

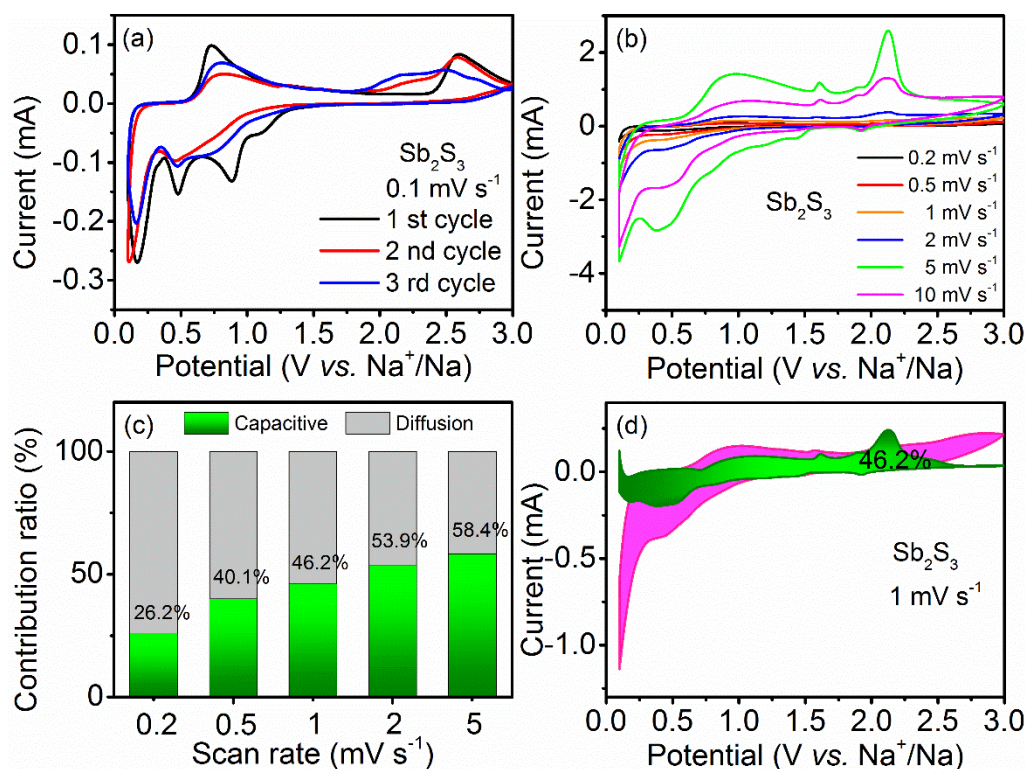


Figure S11. The CV curves at a scan rate of 0.1 mV s^{-1} during the initial three cycles (a), and at different scan rates (b) for Sb_2S_3 composite. The proportion of capacity contribution at different scan rates (c) and the CV curves with the pseudocapacitive contribution at 1.0 mV s^{-1} (d) for Sb_2S_3 electrode.

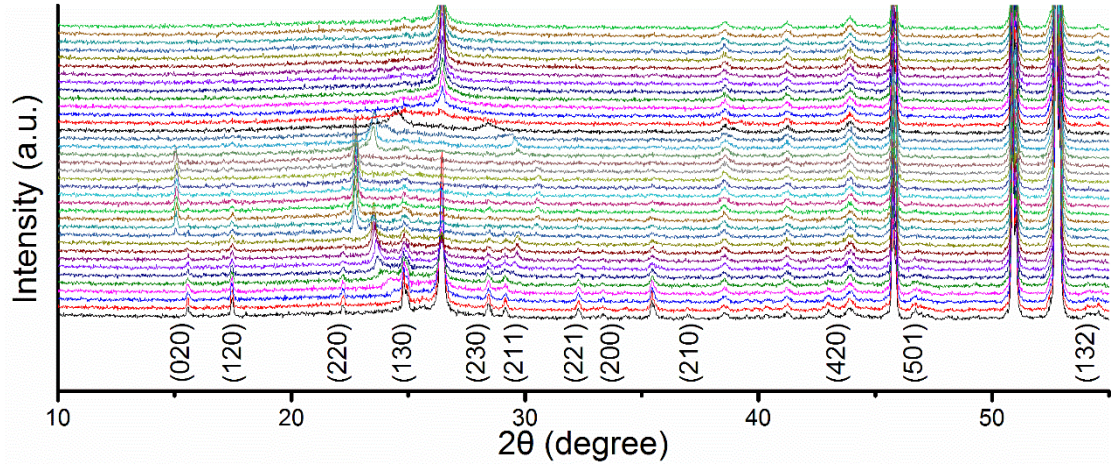


Figure S12. Stacked *in-situ* XRD patterns during the first cycle for SFS/C composite.

Table S2. Fitting results of EIS in Figure 5 with the proposed equivalent circuit.

Samples	$R_s(\Omega)$	$R_{ct}(\Omega)$	$\sigma(\Omega\text{cm}^2\text{s}^{-1/2})$	$D_{Na^+}(\text{cm}^2\text{s}^{-1})$
Sb_2S_3	9.869	15.99	118.21	3.34×10^{-15}
SFS	9.185	11.88	95.72	5.09×10^{-15}
SFS/C	8.598	5.98	54.63	1.63×10^{-14}

R_s represents the series resistance, R_{ct} indicates the charge-transfer resistance and CPE expresses the constant phase element.

Equations S1, S2.

$$D_{Na^+} = \frac{R^2 T^2}{2n^4 F^4 A^2 C^2 \sigma^2} \quad (\text{S1})$$

$$Z' = R_s + R_{ct} + \sigma \omega^{-1/2} \quad (\text{S2})$$

Where R , T , A , F , n , C and σ_w represent the gas constant, absolute temperature, electrode surface area, Faraday's constant, number of electron transform per molecule, the insertion/extraction Na^+ concentration and Warburg factor, respectively.

Table S3. Energetic results of Na₂S adsorption for Sb₂S₃@FeS₂ and pure Sb₂S₃. (Na atom: large yellow sphere, Sb atom: shallow orange sphere, S atom: dark orchid sphere, Fe atom: cyan sphere).

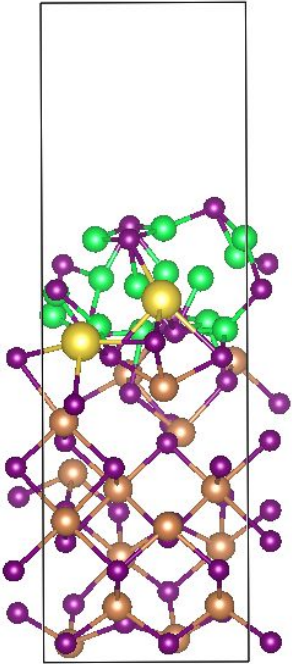
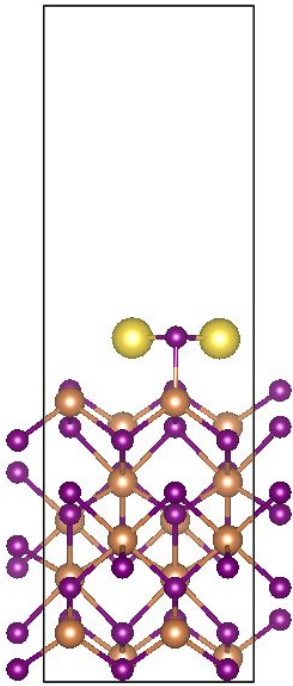
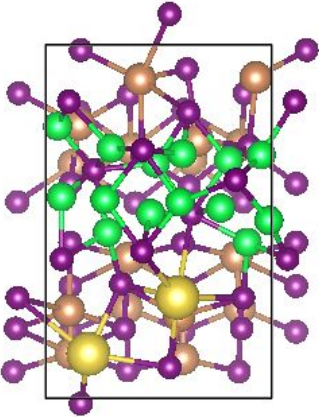
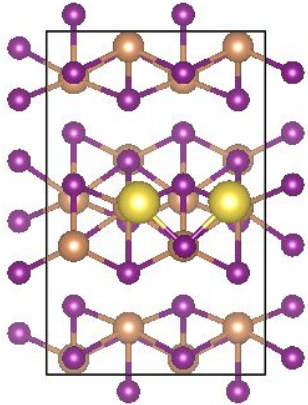
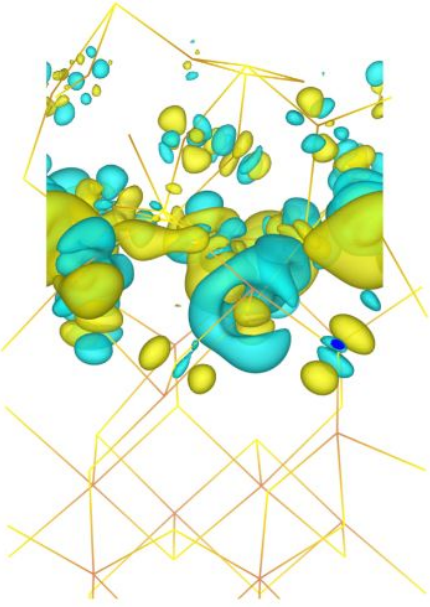
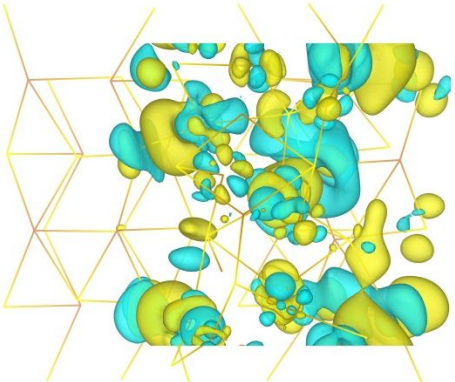
	Sb ₂ S ₃ @FeS ₂	Sb ₂ S ₃
E_{ads}	-1.34 eV	-0.50 eV
Side view		
Top view		

Table S4. Difference charge density analysis of $\text{Sb}_2\text{S}_3@\text{FeS}_2$.

$\text{Sb}_2\text{S}_3@\text{FeS}_2$	
Side view	Top view
	

The total charge density of both Sb_2S_3 and $\text{Sb}_2\text{S}_3@\text{FeS}_2$ shows similar charge density distribution on the Sb-S plane. While the difference charge density of $\text{Sb}_2\text{S}_3@\text{FeS}_2$ exhibits the obvious change in electron density, suggesting the strong interaction between Sb_2S_3 and FeS_2 .

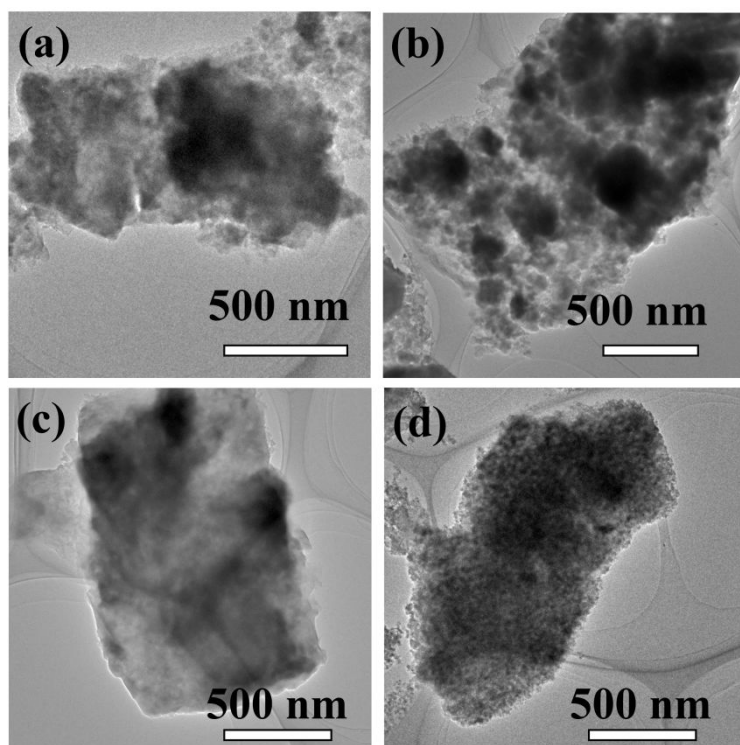


Figure S13. The TEM images of SFS/C electrode at different potential states during the initial (de)sodiation process: discharged to 0.8 V (a) and 0.1 V (b), charged to 1.4 V (c) and 3.0 V (d).

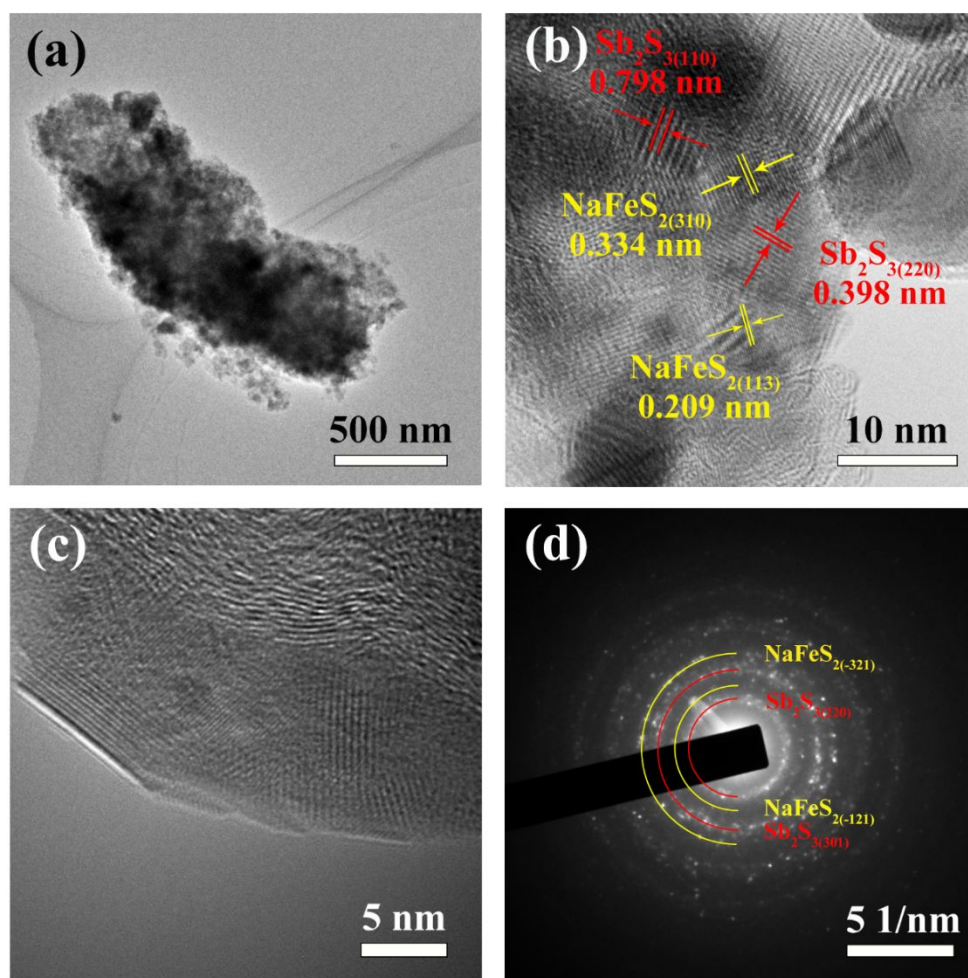


Figure S14. The TEM (a), magnified TEM (b), HRTEM (c) and SAED (d) images of the SFS/C electrodes after 100 cycles at a current density of 0.5 A g⁻¹.

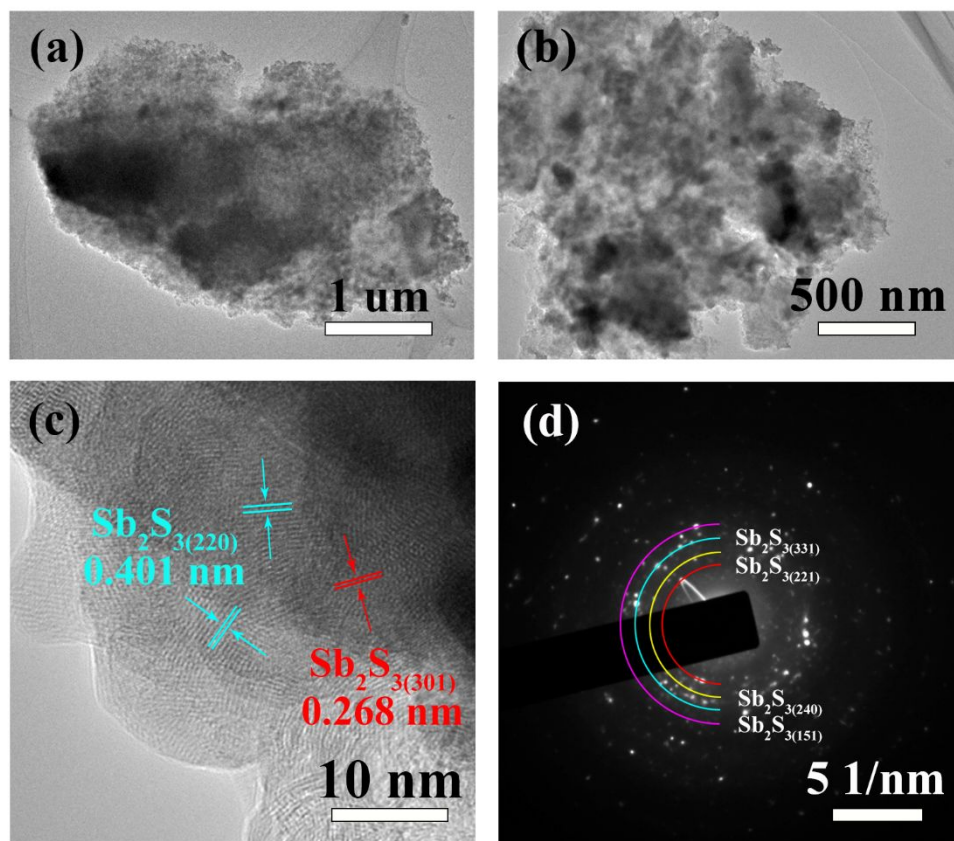


Figure S15. The TEM (a), magnified TEM (b), HRTEM (c) and SAED (d) images of the Sb_2S_3 electrode after 100 cycles at a current density of 0.5 A g^{-1} .

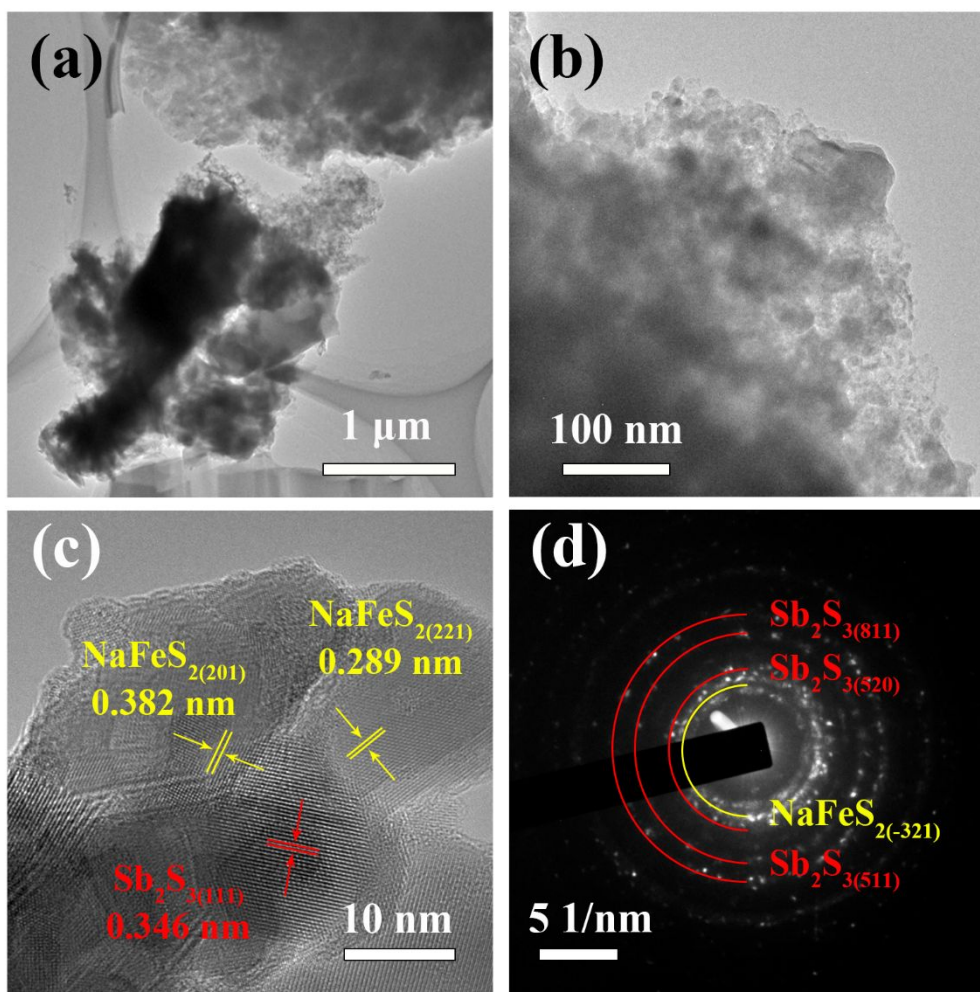


Figure S16. The TEM (a), magnified TEM (b), HRTEM (c) and SAED (d) images of the SFS electrode after 100 cycles at a current density of 0.5 A g⁻¹.

REFERENCES

- S1. Wang, S.; Yuan, S.; Yin, Y.-B.; Zhu, Y.-H.; Zhang, X.-B.; Yan, J.-M. Green and Facile Fabrication of MWNTs@Sb₂S₃@PPy Coaxial Nanocables for High-Performance Na-Ion Batteries. *Part. Part. Syst. Char.* **2016**, *33*, 493-499.
- S2. Pan, Z.-Z.; Yan, Y.; Cui, N.; Xie, J.-C.; Zhang, Y.-B.; Mu, W.-S.; Hao, C. Ionic Liquid-Assisted Preparation of Sb₂S₃/Reduced Graphene Oxide Nanocomposite for Sodium-Ion Batteries. *Adv. Mater. Interfaces* **2018**, *5*, 1701481.
- S3. Cho, J. S.; Park, J. S.; Kang, Y. C. Porous FeS Nanofibers with Numerous Nanovoids Obtained by Kirkendall Diffusion Effect for Use as Anode Materials for Sodium-Ion Batteries. *Nano Res.* **2017**, *10*, 897-907.
- S4. Dong, S.; Li, C.; Ge, X.; Li, Z.; Miao, X.; Yin, L. ZnS-Sb₂S₃@C Core-Double Shell Polyhedron Structure Derived from Metal-Organic Framework as Anodes for High Performance Sodium Ion Batteries. *ACS Nano* **2017**, *11*, 6474-6482.
- S5. Wang, S.; Liu, S.; Li, X.; Li, C.; Zang, R.; Man, Z.; Wang, G. SnS₂/Sb₂S₃ Heterostructures Anchored on Reduced Graphene Oxide Nanosheets with Superior Rate Capability for Sodium-Ion Batteries. *Chem. - Eur. J.* **2018**, *24*, 3873-3881.
- S6. Zheng, T.; Li, G.; Zhao, L.; Shen, Y. Flowerlike Sb₂S₃/PPy Microspheres Used as Anode Material for High-Performance Sodium-Ion Batteries. *Eur. J. Inorg. Chem.* **2018**, *10*, 1224-1228.
- S7. Zhang, Z.; Zhao, J.; Xu, M.; Wang, H.; Gong, Y.; Xu, J. Facile Synthesis of Sb₂S₃/MoS₂ Heterostructure as Anode Material for Sodium-Ion Batteries. *Nanotechnology* **2018**, *29*, 335401.

- S8. Li, J.; Yan, D.; Zhang, X.; Hou, S.; Li, D.; Lu, T.; Yao, Y.; Pan, L. *In Situ* Growth of Sb₂S₃ on Multiwalled Carbon Nanotubes as High-Performance Anode Materials for Sodium-Ion Batteries. *Electrochim. Acta* **2017**, *228*, 436-446.
- S9. Hou, H.; Jing, M.; Huang, Z.; Yang, Y.; Zhang, Y.; Chen, J.; Wu, Z.; Ji, X. One-Dimensional Rod-Like Sb₂S₃-Based Anode for High-Performance Sodium-Ion Batteries. *ACS Appl. Mater. Interfaces* **2015**, *7*, 19362-19369.
- S10. Choi, J.-H.; Ha, C.-W.; Choi, H.-Y.; Shin, H.-C.; Park, C.-M.; Jo, Y.-N.; Lee, S.-M. Sb₂S₃ Embedded in Amorphous P/C Composite Matrix as High-Performance Anode Material for Sodium Ion Batteries. *Electrochim. Acta* **2016**, *210*, 588-595.
- S11. Yao, S.; Cui, J.; Lu, Z.; Xu, Z.-L.; Qin, L.; Huang, J.; Sadighi, Z.; Ciucci, F.; Kim, J.-K. Unveiling the Unique Phase Transformation Behavior and Sodiation Kinetics of 1D van der Waals Sb₂S₃ Anodes for Sodium Ion Batteries. *Adv. Energy Mater.* **2017**, *7*, 1602149.
- S12. Yu, D. Y. W.; Prihodchenko, P. V.; Mason, C. W.; Batabyal, S. K.; Gun, J.; Sladkevich, S.; Medvedev, A. G.; Lev, O. High-Capacity Antimony Sulphide Nanoparticle-Decorated Graphene Composite as Anode for Sodium-Ion Batteries. *Nat. Commun.* **2013**, *4*, 2922.
- S13. Hwang, S. M.; Kim, J.; Kim, Y.; Kim, Y. Na-Ion Storage Performance of Amorphous Sb₂S₃ Nanoparticles: Anode for Na-Ion Batteries and Seawater Flow Batteries. *J. Mater. Chem. A* **2016**, *4*, 17946-17951.